Landau–Zener–Stückelberg interference in a multi-anticrossing system*

Chen Jin-Dan(陈劲丹)[a)], Wen Xue-Da(温学达)[a)],
Sun Guo-Zhu(孙国柱)[b)], and Yu Yang(于 扬)[a)†]

[a)] *National Laboratory of Solid State Microstructures and Department of Physics, Nanjing University, Nanjing* 210093, *China*
[b)] *Research Institute of Superconductor Electronics, Department of Electronic Science and Engineering, Nanjing University, Nanjing* 210093, *China*

(Received 27 December 2010; revised manuscript received 29 January 2011)

We propose a universal analytical method of studying the dynamics of a multi-anticrossing system subjected to driving by a single large-amplitude triangle pulse, within a time scale smaller than the dephasing time. Our approach can explain the main features of the Landau–Zener–Stückelberg interference patterns recently observed in a tripartite system [*Nature Communications* **1** 51 (2010)]. In particular, we focus on the effect of the size of the anticrossing on interference and compare the calculated interference patterns with numerical simulations. In addition, a Fourier transform of the patterns can extract the information about the energy level spectrum.

Keywords: anticrossing, Landau–Zener transition, coherent dynamics

PACS: 85.25.Cp, 03.67.Lx **DOI:** 10.1088/1674-1056/20/8/088501

1. Introduction

Landau–Zener (LZ) transitions[1−3] at the anticrossings play a fundamental role in coherent quantum control, which is key to the realization of quantum computation.[4] To date, much effort has been made to investigate the coherent quantum dynamics of the states at energy-level crossings. In a strongly harmonic-driven two-level system (TLS), repeated LZ transitions give rise to Stückelberg or Ramsey-type oscillations, in analogy to a Mach–Zehnder (MZ) interferometer. The MZ-type interferometry has been observed in a driven superconducting flux qubit,[5] a Cooper–Pair box,[6] and a quantum dot system.[7] These patterns have been theoretically reconstructed from different perspectives.[8−11]

In addition to Landau–Zener–Stückelberg (LZS) interference of one-anticrossing type, several experiments have also reported LZS interference in a multi-anticrossing level structure. In the presence of much stronger harmonic excitation, the qubit state can be driven through more constituent energy-level anticrossings, and the resulting LZS interference reveals complex checkerboardlike patterns.[12] This has been explained well in theory.[13,14] Most recently, a new method of coherent manipulation of quantum states in a tripartite quantum system formed by a superconducting qubit coupled to two TLSs has been reported in Ref. [15]. The manipulation relies on the LZS interference produced by transitions at the two anticrossings, and has a potential application to the precise control of quantum states in the tripartite system. Nevertheless, a universal model to explain the observation has not been proposed. We will show below that it can be understood rather easily using our approach.

In this work, we start with a strongly driven one-anticrossing system where we consider LZ transition as a gate operation. We then analyse the dynamics of a multi-anticrossing system. Under the strong triangle pulse driving, the occupation probability of the system at the initial state exhibits, as a function of driving amplitude and pulse width, diverse LZS interference patterns. Our approach presents a unified analytical treatment of these diverse patterns. In a specific case of two-anticrossing system, we focus on how the interference patterns are influenced by the sweep rate and the coupling strength, thereby elucidating the physics behind the various patterns. Converting the patterns into the phase domain, Fourier transform of the re-

*Project supported by the State Key Program for Basic Research of China (Grant No. 2006CB921801), the National Natural Science Foundation of China (Grant No. 10725415), and the Natural Science Foundation of Jangsu Province, China (Grant No. BK2010012).

†Corresponding author. E-mail: yuyang@nju.edu.cn

© 2011 Chinese Physical Society and IOP Publishing Ltd

sulting population oscillation reveals Fourier components of the compound pattern, which is consistent with our analysis. In all the systems under study, the influence of relaxation and dephasing is neglected to obtain a clear physics picture of the underlying quantum physics.

This paper is organized as follows. In Section 2, we introduce an analytical expression to describe the dynamics for the multi-anticrossing system. In Section 3, we apply the general result to the $N = 2$ case, and focus on the effect of the size of anticrossings on the interference pattern. The calculated patterns of four representative combinations of two anticrossings are in accordance with the numerical results. The discussion of the formation of the interesting dark state–one special structure in the two-anticrossing system, is also included. In Section 4, Fourier transform of these patterns is presented, exhibiting an explicitly ordered structure of one-dimensional arcs that offers energy spectrum information. Finally, Section 5 contains a summary of this work.

2. Model and method

First, we consider one anticrossing system in which two energy levels of a quantum TLS "cross" each other as some external parameter is varied. At the energy-level crossing, the hybridization of the two states results in an anticrossing due to coupling of the states, as shown in Fig. 1(a). The Hamiltonian of TLS is

$$H_{\rm TLS} = \begin{bmatrix} \epsilon_0(t) & \Delta \\ \Delta & \epsilon_1(t) \end{bmatrix}, \tag{1}$$

where $\epsilon_0(t)$ and $\epsilon_1(t)$ are the energy levels of two diabatic states, and Δ is their coupling strength. The transition between energy levels at the anticrossing is what we call LZ transition.

Following Damski and Zurek's adiabatic-impulse approximation model,[3,16] we can obtain a convenient description of the system's dynamics. It is provided that the system evolves adiabatically everywhere except at the point of minimum energy splitting where a sudden mixing in the population of the two energy levels occurs. This non-adiabatic transition at the anticrossing can be described by a unitary transformation[3,6]

$$\hat{U}_1 = \begin{bmatrix} \cos(\theta/2)\exp(-\mathrm{i}\tilde{\phi}_{\rm S}) & \mathrm{i}\sin(\theta/2) \\ \mathrm{i}\sin(\theta/2) & \cos(\theta/2)\exp(\mathrm{i}\tilde{\phi}_{\rm S}) \end{bmatrix}, \tag{2}$$

where $\sin^2(\theta/2) = P_{\rm LZ}$, with $P_{\rm LZ}$ being the Landau–Zener transition probability at the anticrossing. If the anticrossing is swept from the infinity on one side to the infinity on the other, $P_{\rm LZ}$ has the asymptotic form as

$$P_{\rm LZ} = \exp\left(-2\pi\frac{\Delta^2}{\hbar\nu}\right), \tag{3}$$

where $\nu = \mathrm{d}(\epsilon_1 - \epsilon_0)/\mathrm{d}t$ is the variation rate of the energy separation between the two diabatic levels, and 2Δ is the size of the anticrossing. In addition, phase jump $\tilde{\phi}_{\rm S} = \phi_{\rm S} - \pi/2$, which is related to the general Stokes phenomenon,[3] with $\phi_{\rm S}$ being the so-called Stokes phase that takes the form

$$\phi_{\rm S} = \frac{\pi}{4} + \delta(\ln\delta - 1) + \arg\Gamma(1 - \mathrm{i}\delta). \tag{4}$$

where $\delta = \Delta^2/\hbar\nu$ is called an adiabatic parameter, and Γ is the gamma function. In the adiabatic limit, $\phi_{\rm S} \to 0$, and in the sudden limit, $\phi_{\rm S} \to \pi/4$.

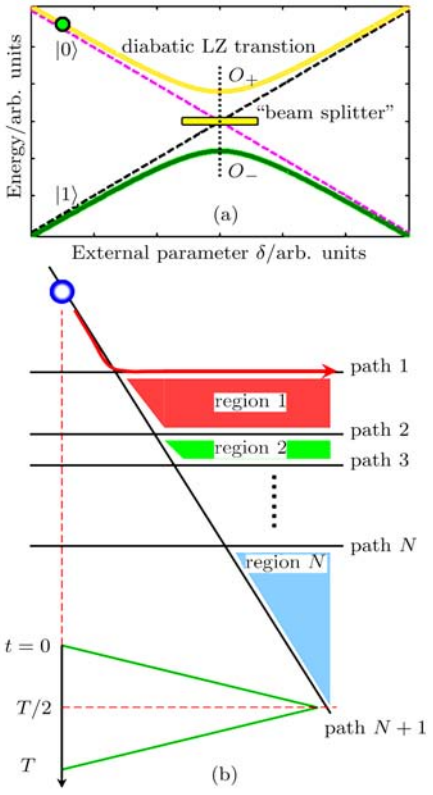


Fig. 1. Schematic diagram of (a) one anticrossing and (b) LZS interference in a phase qubit coupled to N TLSs. (a) the LZ transition at the anticrossing splits the initial state into a superposition of two states in a like manner of a beam splitter. (b) Starting at the dot maker, the qubit state is swept by a triangle pulse. A succession of LZ transitions at the chain of anticrossings results in a superposition state. The state accumulates phases (shaded region), interferes at the return LZ transitions successively, and returns to the initial state with a finite probability.

From the perspective of optics, the avoided level crossing, when driven through, can be viewed as a beam splitter, because LZ transition taking place at the anticrossing splits an input state into a superposition of two states, just analogous to an optical beam splitter which splits the incident light into two beams. In this sense, we define the reflection coefficient as $|r|^2 = 1 - P_{\rm LZ}$ and the transmission coefficient as $|t|^2 = P_{\rm LZ}$.

Then, we take into account the multi-anticrossing system, which can be realized in a superconducting phase qubit with many TLSs inside its Josephson junction. A phase qubit[17−20] consists of a single current-biased Josephson junction. When biased close to the critical current I_0, the qubit can be treated as a tunable artificial atom with discrete energy levels that exist in a potential energy landscape determined by the circuit design parameters and bias. In the qubit-TLS coupled system, TLS[21−24] is formed in the disordered barrier material, where some atoms can occupy two positions, corresponding to two quantum states.[24] When the energy separation of qubit states equals that of the TLS, resonant tunneling between the states opens up an avoided level crossing in the energy spectrum of qubit, and forms a multi-anticrossing chain (see Fig. 1(b)). Its Hamiltonian takes the form,

$$H_{\rm qubit-NTLSs} = \begin{bmatrix} \epsilon(t) & \Delta_1 & \Delta_2 & \cdots & \Delta_N \\ \Delta_1 & \epsilon_1 & 0 & \cdots & 0 \\ \Delta_2 & 0 & \epsilon_2 & \cdots & 0 \\ \vdots & \vdots & \vdots & \ddots & \vdots \\ \Delta_N & 0 & 0 & \cdots & \epsilon_N \end{bmatrix}. \quad (5)$$

The time-dependent $\epsilon(t)$ is energy spacing between the ground state and the excited state of qubit and ϵ_i $(i = 1, \ldots, N)$ is energy spacing of the i-th TLS. It is assumed that qubit is initially prepared in its excited state, and quantum state transitions are then driven using a triangle pulse with amplitude V and period T. This is a double-passage process in which anticrossing regions are passed twice. The first excursion through the anticrossings coherently divides the signal into N output paths, where the dynamical phase is accumulated in the adiabatic parts of the evolution. Then the second excursion recombines the separated signals via LZ transition, and results in the LZS interference patterns.

The algebra describing this one full driving cycle of triangle pulse is as follows. As the anticrossings are traversed from left to right in turn, according to Eq. (2), the transition amplitude to each output path is

$$A_{\rm out} = \begin{cases} \cos\theta_1 & \text{to path 1,} \\ \sin\theta_1 \cos\theta_2 & \text{to path 2,} \\ \sin\theta_1 \sin\theta_2 \cos\theta_3 & \text{to path 3,} \\ \quad\vdots & \quad\vdots \\ (\prod_{k=1}^{k=i-1} \sin\theta_k)\cos\theta_i & \text{to path } i, \\ \quad\vdots & \quad\vdots \\ (\prod_{k=1}^{k=N-1} \sin\theta_k)\cos\theta_N & \text{to path } N, \\ \prod_{k=1}^{k=N} \sin\theta_k & \text{to path } N+1. \end{cases} \quad (6)$$

The adiabatic evolution is in the form of $\exp(\mathrm{i}\phi_i)$, where ϕ_i denotes the phase accumulated on path i relative to the ground state $|0\rangle$ between the two successive crossings. When the anticrossings are traversed from right to left, the transition amplitude back to the initial state from each path $A_{\rm in}$ equals $A_{\rm out}$. Then after one round of LZS interference, the amplitude for the coupling system remaining in the initial state is

$$\begin{aligned} A_{\rm total} &= \sum_{i=\text{path }1}^{\text{path }N+1} A_{\rm out}(i) A_{\rm in}(i) \exp(\mathrm{i}\tilde{\phi}_i) \\ &= \sum_{i=\text{path }1}^{\text{path }N+1} A_{\rm out}^2(i) \exp(\mathrm{i}\tilde{\phi}_i). \end{aligned}$$

Therefore, the probability for the upper level after one period of triangle pulse is given by

$$\begin{aligned} P_1 &= |A_{\rm total}|^2 \\ &= \sum_{i=1}^{N+1}\sum_{j=1}^{N+1} A_{\rm out}^2(i) A_{\rm out}^2(j) \exp(\mathrm{i}\tilde{\phi}_{ij}). \end{aligned}$$

It can be further simplified into the form

$$\begin{aligned} P_1 = & \sum_{i=1}^{i=N+1} A_{\rm out}^2 \\ & + 2\sum_{i=1}^{N+1}\sum_{j=1}^{j<i} A_{\rm out}^2(i) A_{\rm out}^2(j) \cos\tilde{\phi}_{ij}, \end{aligned} \quad (7)$$

where

$$\tilde{\phi}_{ij} = \tilde{\phi}_i - \tilde{\phi}_j = \sum_{n=j-1}^{n=i-1} \Phi_n \quad (j < i). \quad (8)$$

Here $\Phi_n = \int_{t_n}^{t'_n} [E_{\text{path }n}(t) - E_{\text{path }n+1}(t)]\,\mathrm{d}t$ (at $t = t_n(t'_n)$, the n-th anticrossing is traversed from left (right) to right (left)) is the interference phase accumulated in the area of region n, as shown in Fig. 1(b).

Equation (7) indicates that the resulting interference pattern is subjected to the LZ transition amplitude and the interference phase. Every two paths in the energy diagram accumulate one interference phase

and give rise to one type of interference fringe (see Fig. 1(b)). The weightings of the C_{N+1}^2 interference patterns governed by a single phase difference on the resultant interference depends on the LZ transition amplitude. The two factors to determine the LZ transition probability are the size of the anticrossing and the velocity with which it is traversed. Therefore by varying the sweep rate and coupling strength between qubit and TLSs, we can generate a variety of interference patterns with promising use in quantum control.

For example, i) $\sin\theta_k \simeq 0$, which means that the size of the k-th anticrossing is so large that no ingredient of the wavefunction can transmit through it. Therefore, for $i > k$, $A_{\rm out}(i) = 0$, and the number of interferences reduces from C_{N+1}^2 to C_k^2. In particular, if $k = 2$, there is totally $C_2^2 = 1$ interference, i.e., the interference between path 1 and path 2. ii) $\cos\theta_k \simeq 0$, which means that the size of the k-th anticrossing is so small that the wavefunction cannot feel its existence. In this case, $A_{\rm out}(k) = 0$, and the k-th path will not participate in the interference. More interesting concrete examples will be discussed in Section 3.

3. Application to two anticrossings

LZS interference in a phase qubit coupled to two TLSs has recently been observed.[15] A three-dimensional view of the probability of the initial state of qubit under one round of strong triangle pulse driven explicitly characterizes the sweep-rate-dependency of LZS interference. This feature can be explained using the above result applied to the $N = 2$ case. In this case, the coupled Hamiltonian is

$$H_{\rm qubit-2TLSs} = \begin{bmatrix} \epsilon(t) & \Delta_1 & \Delta_2 \\ \Delta_1 & \epsilon_1 & 0 \\ \Delta_2 & 0 & \epsilon_2 \end{bmatrix}. \tag{9}$$

According to the general formula in Eq. (7), the occupation probability at the initial state $|1g_1g_2\rangle$ after one pulse driving takes the form

$$\begin{aligned} P_1 = {} & \cos^4\theta_1 + \sin^4\theta_1\cos^4\theta_2 + \sin^4\theta_1\sin^4\theta_2 \\ & + 2\sin^2\theta_1\cos^2\theta_2\cos^2\theta_1\cos\Phi_{\rm I} \\ & + 2\sin^4\theta_1\sin^2\theta_2\cos^2\theta_2\cos\Phi_{\rm II} \\ & + 2\sin^2\theta_1\sin^2\theta_2\cos^2\theta_1\cos(\Phi_{\rm I}+\Phi_{\rm II}), \end{aligned} \tag{10}$$

where Φ_i (i = I, II) is the total phase accumulated in region i, as shown in Fig. 2. This clearly shows that the interference fringes comprised 3 (C_3^2) patterns, governed by phase accumulation in areas I, II, and I+II, respectively. With the size of the two anticrossings fixed, as the sweep rate is varied, the interference pattern can be divided into three regions displaying the features of the three phase patterns, respectively. In the slow limit, $\rm TLS_1$ acts as a beam splitter and $\rm TLS_2$ acts as a total reflection mirror; the $\Phi_{\rm I}$ pattern dominates. In the fast limit, $\rm TLS_1$ acts as a total transmission mirror and $\rm TLS_2$ acts as a beam splitter; the $\Phi_{\rm II}$ pattern makes the main contribution. In the intermediate region, both $\rm TLS_1$ and $\rm TLS_2$ act as beam splitters; the $\Phi_{\rm I}+\Phi_{\rm II}$ pattern shows the principal feature.

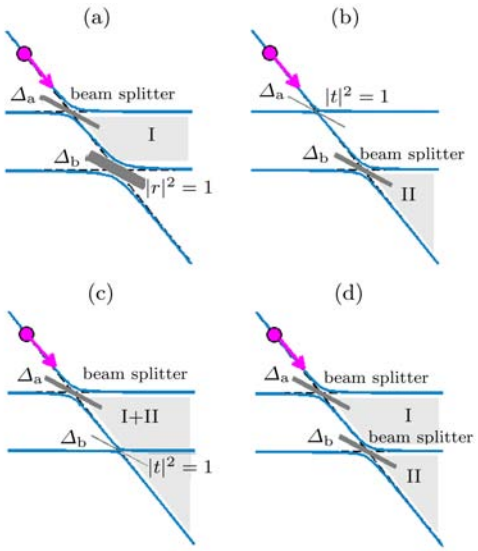


Fig. 2. Different combinations of two beam-splitters. (a) $\Delta_{\rm a} < \Delta_{\rm b}$. $\rm M_1$ acts as a beam splitter, while $\rm M_2$ reflects the state with $P_{\rm LZ}$ approaching zero. Thus the interfering pattern is mainly dependent on the phase accumulated in region I. (b) We still set $\Delta_{\rm a} < \Delta_{\rm b}$, but both of them are much smaller so that $\rm M_1$ transmits the state with $P_{\rm LZ}$ approaching unity, while $\rm M_2$ plays the role of a beam splitter. The phase accumulated in region II plays a major role in forming the interference fringes. (c) $\Delta_{\rm a} > \Delta_{\rm b}$. $\rm M_1$ acts as a beam splitter, while $\rm M_2$ transmits the state. The phase accumulated in regions I+II plays the leading part. (d) $\Delta_{\rm a} = \Delta_{\rm b}$, both $\rm M_1$ and $\rm M_2$ act as beam splitters. $\Phi_{\rm I}, \Phi_{\rm II}$, $(\Phi_{\rm I}+\Phi_{\rm II})$ altogether contribute to the interference pattern.

On the other hand, the size of anticrossing also manipulates the weights of the three patterns in the resulting compound interference fringes. Though the experimental realization of coupling strength control has not been achieved, investigation into the effect of the size of anticrossings on the interference patterns could make predictions of various interference fringes with potential use in future coherent control of a hybrid qubit system. Here we choose four representative combinations of two TLSs, and the parameters used are extracted from Sun's experiment.[15] Based on this, we discuss the effect of Δ below.

(i) $\Delta_a = 10$ MHz, $\Delta_b = 100$ MHz. In this case, $P_{LZ2} \sim 0$, $\sin\theta_2 \sim 0$, $\cos\theta_2 \sim 1$. The occupation probability approximately equals

$$P_1 = \sin^4\theta_1 + \cos^4\theta_1 + 2\sin^2\theta_1\cos^2\theta_1\cos\Phi_I. \quad (11)$$

This combination reveals the main feature of Φ_I pattern.

(ii) $\Delta_a = 1$ MHz, $\Delta_b = 10$ MHz. In this case, $P_{LZ1} \sim 1$, $\sin\theta_1 \sim 1$, $\cos\theta_1 \sim 0$. The occupation probability approximately equals

$$P_1 = \sin^4\theta_2 + \cos^4\theta_2 + 2\sin^2\theta_2\cos^2\theta_2\cos\Phi_{II}. \quad (12)$$

This combination reveals the main feature of Φ_{II} pattern.

(iii) $\Delta_a = 10$ MHz, $\Delta_b = 1$ MHz. In this case, $P_{LZ2} \sim 1$, $\sin\theta_2 \sim 1$, $\cos\theta_2 \sim 0$. The occupation probability approximately equals

$$P_1 = \sin^4\theta_1 + \cos^4\theta_1 + \\ +2\sin^2\theta_1\cos^2\theta_1\cos(\Phi_I + \Phi_{II}). \quad (13)$$

This combination reveals the main feature of $\Phi_I + \Phi_{II}$ pattern.

(iv) $\Delta_a = \Delta_b = 10$ MHz. The occupation probability is in the form of Eq. (10).

Provided that LZ transition probability takes the asymptotic form in Eq. (3), interference patterns in the above 4 cases calculated based on Eq. (10) (see Figs. 3(a)–3(d)) are consistent with the numerical simulations (see Figs. 3(e)–3(h)), except for the slight modulation in one interference fringe involved in the numerical results. The modulation is caused by the fluctuation of actual LZ transition probabilities around its asymptotic form.[15]

In addition, it is noticeable that in a qubit-two-TLSs hybrid system, it is completely possible for a smaller anticrossing to be screened by a larger one, as shown in Fig. 4(a). Although the LZS interference is just the same as that of a single anticrossing, one branch in the spectrum is always in an excited state of TLS, $|TLS1\rangle$ (see the horizontal line in Fig. 4(b)). The system simplified Hamiltonian in a basis formed by $|1g_1g_2\rangle, |0e_1g_2\rangle, |0g_1e_2\rangle$ reads

$$\hat{H}_D = \begin{bmatrix} \omega & \Omega_1/2 & \Omega_2/2 \\ \Omega_1/2 & 0 & 0 \\ \Omega_2/2 & 0 & 0 \end{bmatrix}, \quad (14)$$

where ω is the detuning between qubit and TLS. The eigenstate corresponding to the particular branch is

$$|\Phi_D\rangle = \frac{\Omega_2}{\sqrt{\Omega_1^2+\Omega_2^2}}|0e_1g_2\rangle - \frac{\Omega_1}{\sqrt{\Omega_1^2+\Omega_2^2}}|0g_1e_2\rangle. \quad (15)$$

No ingredient of $|1g_1g_2\rangle$ appears in Eq. (15), and the state $|\Phi_D\rangle$ is analogous to the dark state in quantum optics, in which there is no ingredient of excited state.

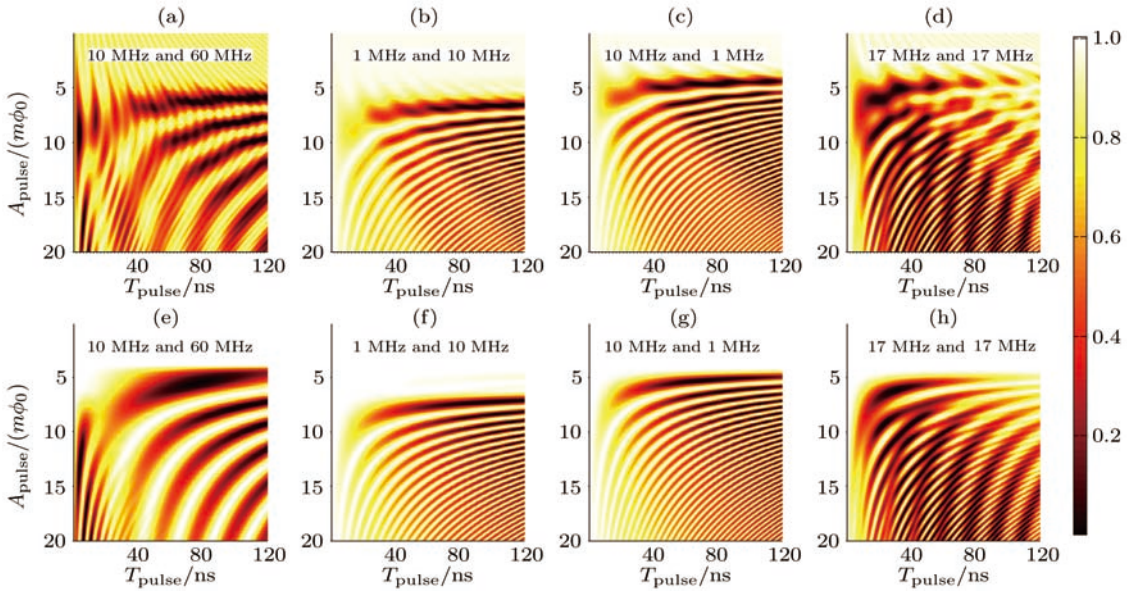


Fig. 3. Panels (a)–(d) are numerical simulations of the qubit population at the initial state $|1\rangle$, each of which is plotted as a function of the amplitude of the driving triangle pulse A_{pulse} and its time width T_{pulse}. Panels (e)–(h) are analytical results using Eq. (10). The parameters used are extracted from our pertinent experiment.[15] (a) and (e) $\Delta_a = 10$ MHz, $\Delta_b = 60$ MHz; (b) and (f) $\Delta_a = 1$ MHz, $\Delta_b = 10$ MHz; (c) and (g) $\Delta_a = 10$ MHz, $\Delta_b = 1$ MHz; (d) and (h) $\Delta_a = \Delta_b = 17$ MHz.

In this sense, we can call it the "dark state of a hybrid qubit". The vacancy of the $|1g_1g_2\rangle$ state could largely reduce the influence of environment on the dark state, and thereby it has a potential application in information storage. The specific method to realize this needs further investigation.

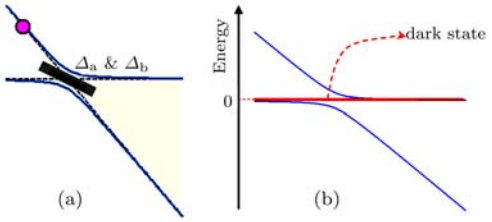


Fig. 4. Dark state in a hybrid qubit. (a) Two TLSs share the same location in the energy diagram, and (b) calculated energy spectrum obtained from Hamiltonian (14). The branch represented by the horizontal line keeps in the state $|\mathrm{TLS1}\rangle$.

4. Fourier transform

Furthermore, Fourier transform (FT) is a helpful tool in identifying the individual phase components of the compound LZS interference. Supposing that the two-anticrossing system follows a linear ramp traversing the anticrossing regions, the FT of the occupation probability in Eq. (10) is found to be

$$\begin{aligned} & P_{\mathrm{FT}}(k_{\mathrm{T}}, A_{\mathrm{pulse}}) \\ = \; & B_0 + B_1\delta(k_{\mathrm{T}} - k_{\mathrm{T1}}(A_{\mathrm{pulse}})) \\ & + B_2\delta(k_{\mathrm{T}} - k_{\mathrm{T2}}(A_{\mathrm{pulse}})) \\ & + B_3\delta(k_{\mathrm{T}} - k_{\mathrm{T1}}(A_{\mathrm{pulse}}) - k_{\mathrm{T2}}(A_{\mathrm{pulse}})), \end{aligned} \tag{16}$$

where

$$\begin{aligned} B_0 &= \cos^4\theta_1 + \sin^4\theta_1\cos^4\theta_2 + \sin^4\theta_1\sin^4\theta_2, \\ B_1 &= 2\sin^2\theta_1\cos^2\theta_2\cos^2\theta_1, \\ B_2 &= 2\sin^4\theta_1\sin^2\theta_2\cos^2\theta_2, \\ B_3 &= 2\sin^2\theta_1\sin^2\theta_2\cos^2\theta_1, \\ k_{\mathrm{T1}} &= \epsilon_{12} - \frac{(\epsilon_1+\epsilon_2)\epsilon_{12}}{2sA_{\mathrm{pulse}}}, \\ k_{\mathrm{T2}} &= \frac{(sA_{\mathrm{pulse}}-\epsilon_{12})^2}{2sA_{\mathrm{pulse}}}, \end{aligned}$$

with s being the diabatic energy-level slope, and ϵ_{12} the detuning between the locations of anticrossing I and II.

Therefore, it is expected that FT reveals a highly ordered structure of one-dimensional arcs in Fourier space. (I) Φ_{I} pattern dominates, i.e., $\sin\theta_2 \simeq 0$. In this case, $B_2, B_3 \simeq 0$, and $P_{\mathrm{FT}} \simeq 2\sin^2\theta_1\cos^2\theta_1\delta(k_{\mathrm{T}} - k_{\mathrm{T1}}(A_{\mathrm{pulse}}))$. Apparently, there is only one curve corresponding to $k_{\mathrm{T}} = k_{\mathrm{T1}}$ after FT. (II) Φ_{II} pattern dominates, i.e., $\cos\theta_1 \simeq 0$. In this case, $B_1, B_3 \simeq 0$, and $P_{\mathrm{FT}} \simeq 2\sin^4\theta_1\sin^2\theta_2\cos^2\theta_2\delta(k_{\mathrm{T}} - k_{\mathrm{T2}}(A_{\mathrm{pulse}}))$. Only $k_{\mathrm{T}} = k_{\mathrm{T2}}$ shows up after FT. (III) $\Phi_{\mathrm{I}} + \Phi_{\mathrm{II}}$ pattern dominates, i.e., $\cos\theta_2 \simeq 0$. In this case, $B_1, B_2 \simeq 0$, and $P_{\mathrm{FT}} \simeq 2\sin^2\theta_1\cos^2\theta_1\delta(k_{\mathrm{T}} - k_{\mathrm{T1}}(A_{\mathrm{pulse}}) - k_{\mathrm{T2}}(A_{\mathrm{pulse}}))$. Only $k_{\mathrm{T}} = k_{\mathrm{T3}}$ shows up after FT. (IV) All three patterns, including Φ_{I}, Φ_{II}, and $\Phi_{\mathrm{I}}+\Phi_{\mathrm{II}}$ dominate, i.e., $\sin^2\theta_1 \simeq \sin^2\theta_2 \simeq 1/2$. In this case, $B_1 \simeq B_3 \simeq 1/4$ and $B_2 \simeq 1/8$. All three curves corresponding to $k_{\mathrm{T}} = k_{\mathrm{T1}}$, $k_{\mathrm{T}} = k_{\mathrm{T2}}$, and $k_{\mathrm{T}} = k_{\mathrm{T3}}$ can be observed after FT. This is explicitly demonstrated in Fig. 5, which is based on the discrete Fourier transform method

$$\begin{aligned} & P_{\mathrm{DFT}}(k_{\mathrm{T}}, A_{\mathrm{pulse}}) \\ = & \sum_{j=1}^{N} P_{1j}(T, A_{\mathrm{pulse}})\omega_N^{(j-1)(k-1)}, \end{aligned} \tag{17}$$

where $\omega_N = \exp(-2\pi\mathrm{i}/N), N = 1, 2, \ldots$. As labeled in the figure, different curves correspond to different phase patterns, which is consistent with our above

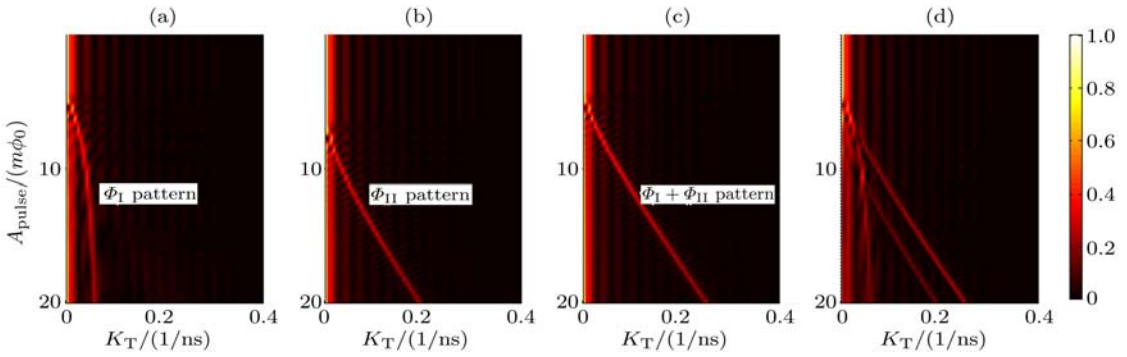


Fig. 5. Discrete Fourier transform of the LZS patterns in Fig. 2. In the FT, one curve corresponds to one interference pattern. The number of curves indicates the number of anticrossings that act as beam splitters under pulse driving. The curves in panels (a)–(c) indicate Φ_{I}, Φ_{II}, $\Phi_{\mathrm{I}}+\Phi_{\mathrm{II}}$ patterns, respectively. Panel (d) shows all three curves as in this case where all the patterns make comparable contributions to the interference.

analyses. In the multi-anticrossing system, if N anticrossings take part in the LZS interference, C_{N+1}^2 phase components can be observed in its FT and *vice versa*. Therefore, the FT provides a means to ascertain how many TLSs are effectively coupled to a qubit.

5. Summary

We present a simple form of analytic expression to describe the coherent dynamics of a driven multi-anticrossing chain. The oscillatory population of the hybrid system remaining in the initial state exhibits a rich pattern of LZS interference in the two-dimensional phase space parameterized by pulse width and driving amplitude. In the N-anticrossing chain, the resulting compound interference is the addition of C_{N+1}^2 patterns governed by two transmitted paths, whose weights rely on the LZ transition amplitude. This is clearly demonstrated by their Fourier transforms of the pulse width, which serve as a useful tool in offering information about the energy spectrum. Although the intrinsically random nature of TLSs precludes the direct control of their distribution and coupling strength by a qubit, our discussion of possible types of special hybrid qubit can be used to understand some observed patterns, and to predict future experimental phenomena, in particular when considering the rapid technological advancement of a macroscopic device with an atomic-sized system.[24] Moreover, it is straightforward to apply our method to a superconducting flux qubit, where resonant tunneling between its double well potentials forms a multi-anticrossing net. Although the effort has been made to study that system,[25] our universal model can give a more general description of the system.

References

[1] Zener C 1932 *Proc. R. Soc. London* A **137** 696

[2] Oliver W D and Valenzuela S O 2009 *Quantum Infor. Process.* **8** 261

[3] Shevchenko S N, Ashhab S and Nori F 2010 *Phys. Rep.* **492** 1

[4] Mooij H 2005 *Science* **307** 1210

[5] Oliver W D, Yu Y, Lee J C, Berggren K K, Levitov L S and Orlando T P 2005 *Science* **310** 1653

[6] Sillanpää M, Lehtinen T, Paila A, Makhlin Y and Hakonen P 2006 *Phys. Rev. Lett.* **96** 187002

[7] Petta J R, Lu H and Gossard A C 2010 *Science* **327** 669

[8] Valenzuela S O, Oliver W D, Berns D M, Berggren K K, Levitov L S and Orlando T P 2006 *Science* **314** 1589

[9] Berns D M, Oliver W D, ValenzuelaS O, Shytov A V, Berggren K K, Levitov L S and Orlando T P 2006 *Phys. Rev. Lett.* **97** 150502

[10] Rudner M S, Shytov A V, Levitov L S, Berns D M, Oliver W D, Valenzuela S O and Orlando T P 2008 *Phys. Rev. Lett.* **101** 190502

[11] Wei L F, Johansson J R, Cen L X, Ashhab S and Nori F 2008 *Phys. Rev. Lett.* **100** 113601

[12] Berns D M, Rudner M S, Valenzuela S O, Berggren K K, Oliver W D, Levitov L S and Orlando T P *Nature* **455** 07262

[13] Wen X and Yu Y 2009 *Phys. Rev.* B **79** 094529

[14] Ferrón A, Domínguez D and Sánchez M J 2010 *Phys. Rev.* B **82** 134522

[15] Sun G, Wen X, Mao B, Chen J, Yu Y, Wu P and Han S 2010 *Nature Commun.* **1** 51

[16] Ashhab S, Johansson J R, Zagoskin A M and Nori F 2007 *Phys. Rev.* A **75** 063414.

[17] Makhlin Y, Schön G and Shnirman A 2001 *Rev. Mod. Phys.* **73** 357

[18] You J Q and Nori F 2005 *Physics Today* **58** 42

[19] Clarke J and Wilhelm F K 2008 *Nature* **453** 1031

[20] Martinis J M 2009 *Quantum Infor. Process.* **8** 81

[21] Simmonds R W, Lang K M, Hite D A, Nam S, Pappas D P and Martinis J M 2004 *Phys. Rev. Lett.* **93** 077003

[22] Martinis J M, Cooper K B, McDermott R, Steffen M, Ansmann M, Osborn K D, Cicak K, Oh S, Pappas D P, Simmonds R W and Yu C C 2005 *Phys. Rev. Lett.* **95** 210503

[23] Zagoskin A M, Ashhab S, Johnansson J R and Nori F 2006 *Phys. Rev. Lett.* **97** 077001

[24] Neeley M, Ansmann M, Bialczak R C, Hofheinz M, Katz N, Lucero E, O'Connell A, Wang H, Cleland A N and Martinis J M 2008 *Nature Physics* **4** 523

[25] Xu S, Yu Y and Sun G 2010 *Phys. Rev.* B **82** 144526.